Computational Analysis of High Lift Generating Airfoils for Diffuser Augmented Wind Turbines

Aniruddha Deepak Paranjape[1], Anhad Singh Bajaj[1], Shaheen Thimmaiah Palanganda[1], Radha Parikh[1], Raahil Nayak[1], and Jayakrishnan Radhakrishnan[1]

1. Department of Aeronautical and Automobile Engineering, Manipal Institute of Technology, Manipal 576104, Karnataka, India.

Correspondence: Jayakrishnan Radhakrishnan (jayakrishnan.r@manipal.edu)

Abstract.

The present study aims to analyze the basic aerodynamic performance of a Diffuser Augmented Wind Turbine (DAWT) using high lift generating airfoils in the diffuser cross-section that encloses the turbine. The study is a Computational Fluid Dynamics (CFD) analysis of the flow across the rotor blades and through the diffuser, which is carried out using Reynolds
5 Averaged Navier-Stokes (RANS) simulations. The rotor blades are modeled as a porous Actuator Disk (AD). Various high-lift generating airfoils are used in the diffuser geometries with additional geometric modifications, such as a flange, are taken into consideration and analyzed for the velocity of the flow at the actuator disk to determine the overall aerodynamic performance of the diffuser shape.

1 Introduction

10 Wind energy is establishing itself as one of the fastest growing sources of renewable energy in the world with approximately 50 GW capacity being installed consistently all over the world since 2014. In 2018, wind energy production reached 591 GW and wind power accounted for almost 6% of the global electricity demand thus making wind energy one of the most promising, effective and dependable sources of renewable energy. Recent predictions by the United Nations regarding global warming calls for the entire global community to shift focus into developing effective renewable energy systems. The abundance of
15 wind all across the globe has caused researchers to focus on a system which can increase power output without a penalty for the size of the wind turbine. While large wind turbines are placed where the wind topology is optimum, smaller wind turbines are locally built to supply power to meet the demands.

A conventional horizontal axis wind turbine (HAWT) represented by an AD has the ability to extract 59.3% of the kinetic energy of the free-stream wind. This is known as the Betz-Joukouwski limit as defined by the Betz law of wind turbine
20 performance. This limit however, can be overcome by some additional 'augmentation' devices. The idea of a Shrouded or Diffuser Augmented Wind Turbine (DAWT) was first explored by Lilley and Rainbird (Lilly and Rainbird, 1956), where they described power augmentation of small shrouded wind turbines as far back as 1956. Since then, numerous studies have been conducted to investigate and optimize the efficiency for a wind turbines through various means. This paper aims to investigate
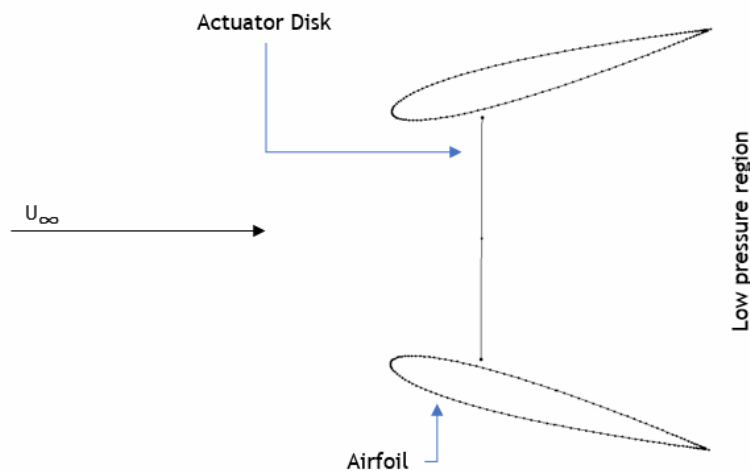
Figure 1. Schematic of the geometry and its orientation to relative velocity U_∞

the effects of high-lift generating airfoils on a DAWT for a turbulent Reynolds number of 5,00,000. A high-lift airfoil improves the aerodynamic efficiency (C_L/C_D) at low speeds by having a high lift coefficient with minimum drag penalties. The thickness has very little effect in determining the maximum lift coefficient of the airfoils. By adding a diffuser, the wake of the turbine blades is allowed to rapidly expand, resulting in a subsequent drop in pressure. This in turn leads to an increase in the mass

5   flow rate of the incoming free stream wind, thereby crossing the Betz-Joukowski limit. Through wind tunnel testing, Igra (Igra, 1981) found that power coefficient could be improved by 80% of that of a conventional wind turbine just by placing a diffuser over it. Abe and Ohya (Ohya et al., 2008), varied the diffuser open angle by adding a flange around the diffuser exit. The study shows that flanged diffusers, that is, the additional geometric modification to the shroud can cause a larger wake expansion due to vortices generated at the tips of the flange. The mass flow rate is further increased by the enhanced low pressure region. In a

10   DAWT, maximum energy can be drawn from a high thrust coefficient AD by increasing the expansion ratio. Nevertheless, this cannot be increased indefinitely as it would cause boundary layer flow separation. Thus, there is an optimum configuration for which the velocity through the AD can be maximized. (Ohya et al., 2008, Aranake and Duraisamy, 2016)

    The turbine is modeled as an AD in the present study and a pressure drop is induced across this disk according to Bernoulli's Theorem. This pressure drop characterizes a change in the velocity field as the particles cross the turbine blades and energy is

15   extracted. The entire flow field can be identified as a two dimensional flow field. The separation effects and flow losses from the tips are assumed to be negligible. In this study, a brute force approach is used on a pool of various high lift generating airfoils. The airfoils are categorized as per their family and tests against different parameters such as area ratio, and effects of a flange

on the diffuser are conducted. These tests were successively performed using CFD simulations to find the best performing airfoils in each family of airfoils (Dighe et al., 2018).

The present numerical study has been carried out using the commercially available computational fluid dynamics (CFD) solver ANSYS® Fluent.

2 Actuator Disk Modeling

5

The purpose of the rotor is to extract kinetic energy from the velocity that impinges on the blades of the rotor. This causes a reduction in velocity of the flow across the blades. This change in kinetic energy invariably causes a thrust force in the direction of the incoming flow. There is also a frictional drag component that is created as a result of the flow over the blades. The resultant torque created due to the rotational motion of the blades also contributes to the change in the kinetic energy of

10 the flow. Thus, wind turbine forces are operated by balancing the thrust force, torque of the blades and kinetic energy of the flow. The AD method is used to model the forces and moments of the rotor system of the turbine blades. The basic idea of an AD is to replace the rotor blades with a permeable disc of equivalent area. The actuator disk uses the mass and momentum conservation principles to balance the applied forces as compared to the axial and tangential momentum equations that balance the applied forces on the real rotor blades. Thus, the AD can be used to conveniently model and assist the calculation of rotor

15 aerodynamics. (Mikkelsen et al., 2004)

The AD exerts a constant thrust T_A, per unit surface. The coefficient is given by (Dighe et al., 2018):

$$C_{T_{AD}} = \frac{T_A}{\frac{1}{1}\rho U^2 S_a}$$

where, ρ is the fluid density, U is the freestream velocity and S_a is the surface area of the AD. The pressure drop across the AD (Δp) is input as a constant during the simulations and the force as $T_A = S_a$ x Δp. Thus, a constant coefficient of thrust can be maintained across the the AD.

The average AD velocity can be found by integrating the freestream velocity in the x-direction over the defined surface area of the AD:

$$U_{AVG} = \frac{1}{S_a} \int \frac{\partial U}{\partial x} dS$$

Using the above results we can define a power coefficient for the duct geometry with an AD of surface area S_a:

$$C_P = \frac{P}{\frac{1}{1}\rho U^2 S_a} = \frac{U_{AVG}}{U} C_{T_{AD}}$$

3 Computational Fluid Dynamics Methodology

3.1 Grid Validation and Independence Studies

20

A grid validation was conducted to verify the accuracy of the mesh, while a grid convergence study was conducted to determine the optimum mesh configuration without sacrificing the accuracy of the result.

For the validation of the mesh that was generated, Igra's (Igra, 1981) experimental wind tunnel set-up was replicated in the numerical domain. Igra carried out a number of experiments during his research on diffuser augmented wind turbines. Of this, his experimental set-up of the 'Circular Wing Shrouds" is considered for the validation study. Similar to the experimental set-up, the numerical domain uses the NACA 4412 airfoil as highlighted in the **Figure 2**. The angle of attack of the airfoils

5 is fixed at $2°$ and the area ratio is maintained at 1.84 for this configuration. Wall blockages and interferences are ignored for the experimental set-up to avoid elaborate wind tunnel corrections. The inflow velocity was maintained at 6 m/s. The results were analysed against experimental pressure distributions and forces.(Dighe et al., 2019) The mesh generated on ICEM CFD showed good compatibility with Igra's experimental results thus proving the validity of the mesh.

Three meshes were used with different number of nodes and elements, in order to optimize the mesh in terms of simulation

10 time. All the meshes had NACA 4412 as the airfoil and were simulated under similar conditions with an inlet velocity of 6m/s.

Table 1: Grid Convergence Study Results

Grid	Number of Elements	Velocity Output (m/s)
Coarse	4776	7.826434
Medium	175291	8.678735
Fine	457512	8.7638

The first mesh was coarse, with roughly 4627 nodes and 4776 elements in total and took 2 minutes to converge. As expected, the mesh gave a very poor result with a velocity of $7.826434 m/s$ at the AD. The second mesh was a fine mesh with a total

15 of roughly 174246 nodes and 175291 elements. This mesh took about 10 minutes for the solution to converge and gave a better and a more accurate result with a velocity of $8.678735 m/s$ at the AD. The third mesh was even finer and had a total of 456031 nodes and 457512 mesh elements. This mesh took about 22 minutes for the solution to converge and gave a velocity of $8.7638 m/s$ at the AD. The finest mesh differed by a 0.98% from the medium quality mesh. Thus the medium quality mesh with 174246 nodes and 175291 elements was chosen, as it was accurate with an added advantage of reduced computational

20 time and power.

3.2 Simulation Domain

To conduct the present study, ANSYS® and its constituent modules were used to generate, simulate, visualize and process the results. ICEM CFD®, ANSYS Inc. was used to generate the mesh required, as it offers great control and flexibility over the grid generation process. The computational domain chosen was a C-Type topography as it is easy to generate and minimizes

25 the skewness of the mesh in the near-wall condition. It also has the ability to accurately simulate the flow at various angles of attack. The geometry consists of two-dimensional planar airfoils symmetrically placed about the central axis along with a rotor modeled as an AD. Following Avallone et al, (Dighe et al., 2019) the tip clearance has been fixed at 2.5% . The free-stream velocity is set as 6 m/s for the present study and the flow is considered to be steady, uniform, incompressible and turbulent for the airfoil chord length. While the simulated conditions are two dimensional, the conditions are sufficient to gain enough

insights due to the axisymmetric nature of the flow. For the given Reynolds number, the Y+ was kept well under 1 in order to calculate the wall spacing assisting the meshing process.
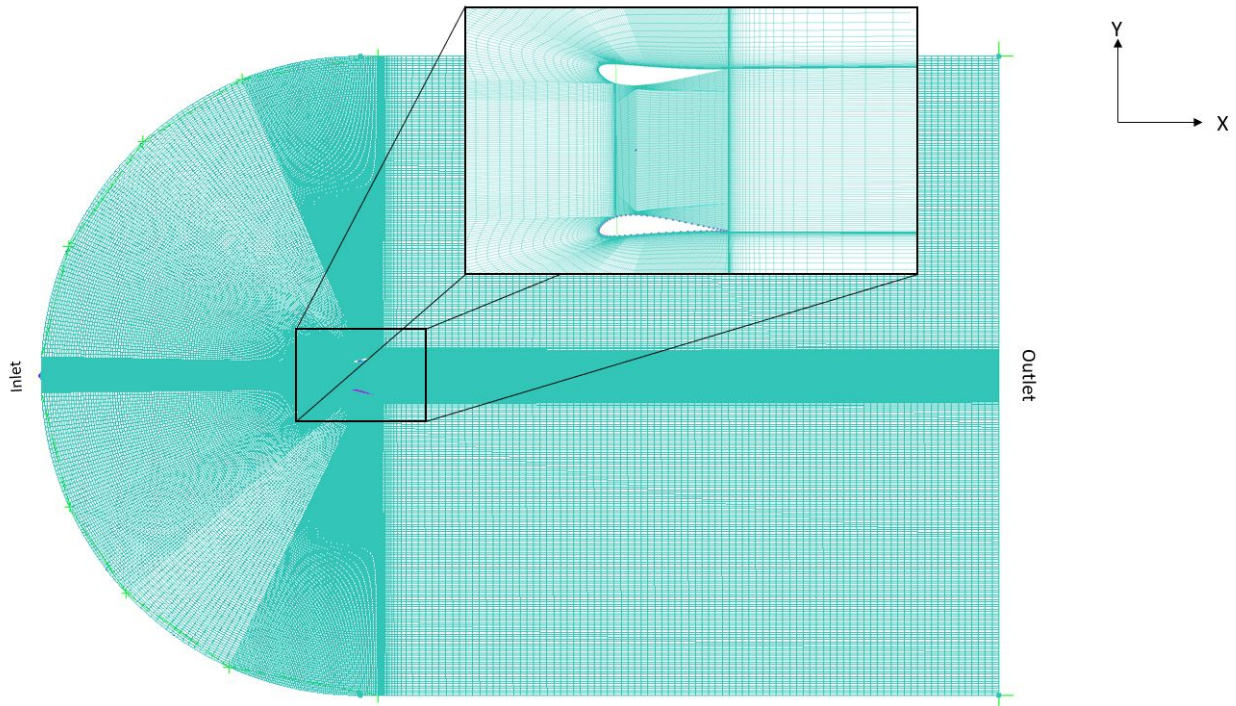

Figure 2. The C-Type topography and detailed look of the duct geometry

ANSYS Fluent® was used as the flow solver, while CFD Post and GNU Octave®, an open source high-level programming language for numerical computations, was used to process the results. A brute force method was used to select and further

5 optimize the design to shortlist the best performing airfoils from the given gene pool. The method is discussed in detail in the section **3.4**.

3.3 Governing equations

To properly model the viscous flows over the various diffuser configurations at turbulent Reynolds numbers, the Navier–Stokes equations are selected in Cartesian coordinate system. The turbulence model used is k-ω Shear Stress Transport (SST) which is

10 expressed as a set of partial differential equations. The k-ω SST, which was developed by Menter, [9] is a two equation robust model for turbulence growth and is one of the most widely used turbulence models. This is because the SST combines the use of $k - \omega$ in near wall flow and $k - \epsilon$ in free shear flow.

The $k - \omega$ SST was introduced by Menter in 1994 to deal with the strong freestream sensitivity of the $k - \omega$ model. It was also aimed at improving the predictions of the model in adverse pressure gradients. The switching of the model between $k - \omega$

and $k - \epsilon$ was achieved by Menter by adding a blender function. The blender function utilises the k-ω model for near wall flow while using k-ϵ for the free-stream flow. This makes the model more accurate and reliable yet computationally more feasible as compared to a Large Eddy Simulations (LES) or Direct Numerical Simulation (DNS), which are computationally more expensive. Over the years the model has undergone several revisions which have greatly improved the models' efficacy. The

5 $k - \omega$ model is known to often over predict turbulence in regions of large normal strain, stagnation points and regions with strong accelerations. Although the model is known to often report higher values of turbulence than normal, the discrepancies are documented and the errors are small in order.

The two equations are often termed as the turbulence kinetic energy and the specific dissipation rate of the eddy viscosity. The governing equations are as follows(Menter et al., 1994):

Kinematic Eddy Viscosity:

$$\nu_{\mathrm{T}} = \frac{a_1 k}{max(a_1 \omega, S F_2)}$$

10

Turbulence Kinetic Energy:

$$\frac{\partial k}{\partial t} + U_{\mathrm{j}} \frac{\partial k}{\partial x_{\mathrm{j}}} = P_{\mathrm{k}} - \beta^* k \omega + \frac{\partial}{\partial x_{\mathrm{j}}} \left[(\nu + \sigma_{\mathrm{k}} \nu_{\mathrm{T}}) + \frac{\partial k}{\partial x_{\mathrm{j}}} \right]$$

Specific Dissipation Rate:

$$\frac{\partial \omega}{\partial t} + U_{\mathrm{j}} \frac{\partial \omega}{\partial x_{\mathrm{j}}} = \alpha S^2 - \beta \omega^2 + \frac{\partial}{\partial x_{\mathrm{j}}} \left[(\nu + \sigma_{\mathrm{w}} \nu_{\mathrm{T}}) + \frac{\partial \omega}{\partial x_{\mathrm{j}}} \right]$$

3.4 Simulation Methodology

The present study aims at exploring different airfoil designs and shapes, in order to optimize the ultimate design of the diffuser within the given constraints. **Figure 3** highlights a genepool of 12 airfoils that have been chosen from 3 different airfoil

15 families, namely, Eppler, NACA and Selig. The airfoils were selected based on their lift-drag ratio for the given turbulent Reynolds number. (Dighe et al., 2018)

In the first stage, the airfoils were fixed at a constant area ratio. The results obtained were compared to the NACA 0012 test case and amongst themselves. RANS equations were utilized in this analysis for maximum simplicity. Based on the results of the first stage of simulations conducted, some of the airfoils were eliminated from each of the families (Igra, 1981). Taking the

20 process forward, the angle of attack of the airfoils and area ratio was varied and the end result was an optimized area ratio for each of the families. The simulations conducted during the second and third stage were all done using a commercial RANS approach. At the end of this stage, some more airfoils were eliminated from the process. The remaining airfoils were then taken with their optimum area ratios and added with a 15° flange at the trailing edge at 70% of the chord to generate vortices that further reduce the pressure in the low pressure region behind the airfoil. The subsequent trends and results were documented

25 and analysed.

Figure 3. The gene pool of high-lift generating airfoils

At present, a constant duct thrust co-efficient is maintained by keeping a constant pressure difference across the AD. The effects of varying the duct thrust is presently beyond the scope of this study. The effects of the tip clearances on the duct performance are also beyond the scope of this study as the tip clearance has been fixed at 2.5%

4   Results and Discussion

5 This section looks into the results of the present study at each stage of the process. For the initial performance of the airfoils in the first stage of the brute force approach, the area ratio was fixed at 1. During this phase, airfoils from each family were eliminated based on its performance with respect to the velocity at the AD. From the results, NACA 63(2)-615, S4110 and E222 were eliminated from the NACA, Selig and Eppler families respectively, leaving 9 airfoils in the genepool, for further analysis and study.

10 The results are plotted on a graph with thickness ratio on the x-axis and velocity on the y-axis. These results are highlighted below and give a clear indication of the best performing airfoils in their respective families as seen in **Figure 4**. The 3 airfoils having the least velocities at the corresponding AD are eliminated in this stage.

For the second stage analysis, the best performing airfoils were taken from the results of stage one, and their angles of attack were varied from $0°$ to $12°$ in steps of $4°$, and subsequently by $1°$ till it reached $20°$. For the initial variations of up to $12°$, the

15 flow remained attached to the surface of the airfoil. No peak value in the velocity at the AD was observed at $0°$. As the angle of attack was increased, an upward trend was noted in the velocity across the AD, as a consequence of increasing the area ratio. The observed decrease in the pressure gradient at the trailing edge of the airfoil allows wake expansion, thereby increasing the velocity of the free stream wind at the AD. The velocity increase at the AD was significant beyond an angle of attack of $12°$.
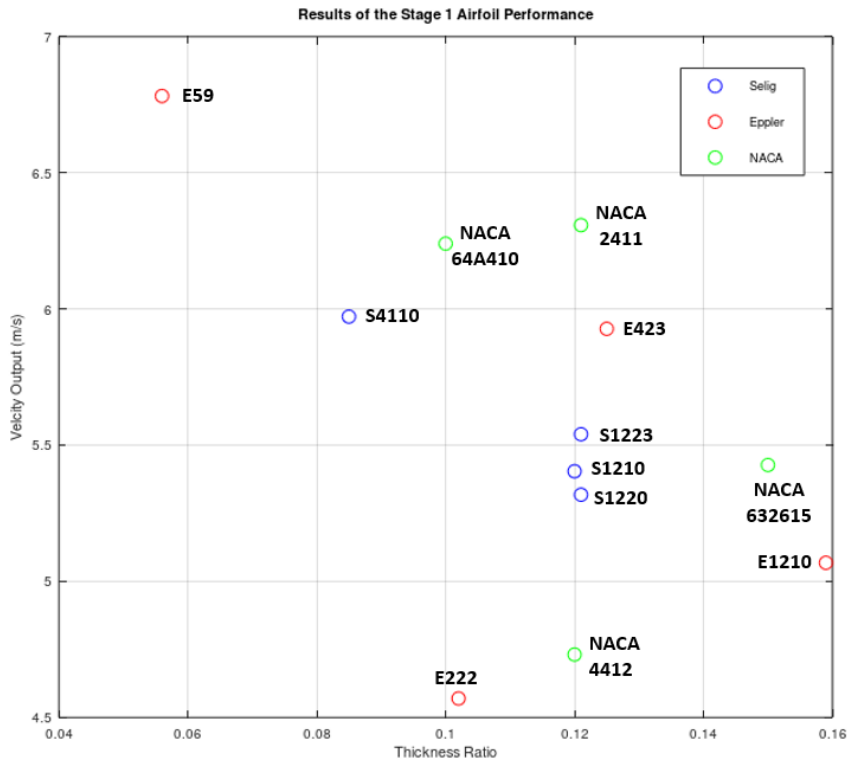
Figure 4. The figure shows the variation of the velocity output of the duct to their thickness ratio

The following table highlights the angles of attack for each family of airfoils at which the respective velocities reached its peak value at the AD.

Table 2: Optimum angles at the end of stage two

Airfoil Family	Optimized Angle
Eppler	15°
NACA	14°
Selig	18°

5   Beyond the above mentioned angles, there was no appreciable rise in the value of the velocity across the AD. It is observed that the flow mostly remains attached to the diffuser, with little flow separation at the trailing edge. Hence, it can be concluded that the values obtained are optimized for the diffusers of the respective families.
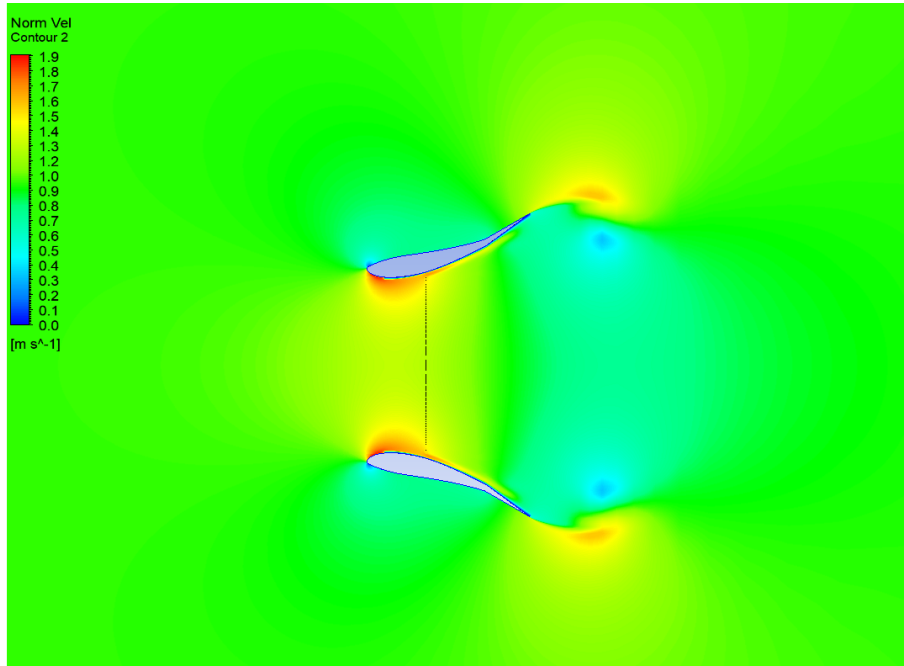
Figure 5. S1210 normalized velocity contour of the result from the second stage of the study

Upon analysing the results of the second stage, the study was taken forward by eliminating the worst performing airfoil from each of the three families. By adding a flange to the trailing edge at an open angle of 15°, as per the study conducted by El-Zahaby et al (El-Zahaby et al., 2016), a further reduction in pressure is observed by virtue of vortices generated at the tip of the flange. This causes an overall increase of the velocity across the AD. In this phase, simulations are carried out with the flange added to the airfoils at 70% of the chord length for the remaining 6 airfoils. The velocity contours from this phase are shown below in **Figure 6**. It is observed that there is almost no flow separation along the airfoil. The generation of vortices in the wake of the diffuser is more pronounced. The reduction in the velocity of the flow in the low pressure region is also significant.

Table 3: Best performing airfoils at the end of stage three

Best Performing Airfoil	Velocity Output (m/s)
NACA 4412	9.216928
Selig 1223	9.410147
Eppler 423	9.432198

Thus, the flange acts as a secondary velocity augmentation device to the present high lift generating airfoil shroud that exists around the AD. It is observed that NACA4412, S1223 and E423 are the best performing airfoils from each of the respective
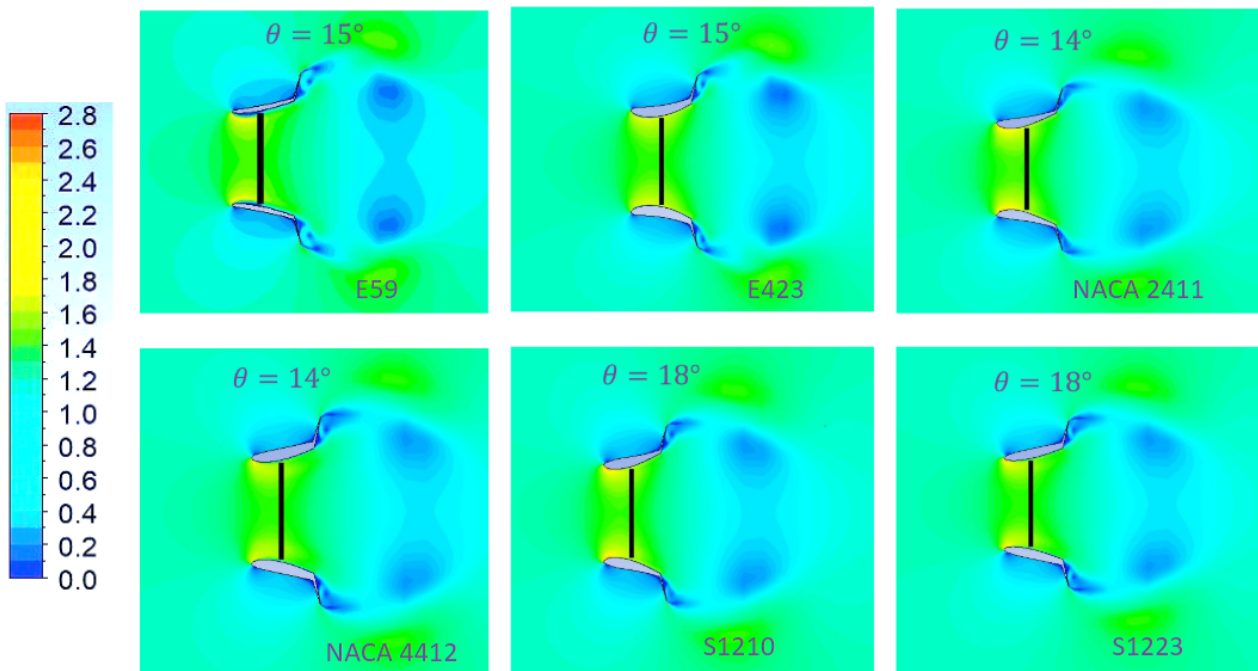
Figure 6. The normalized velocity contours of the 6 best performing airfoils with the flange

families. E423 is the best performing airfoil from the genepool. It is therefore the best suited airfoil to be modeled as a diffuser for the given configuration. To summarize, an investigation into the effects of high lift generating airfoils on the duct geometry that is, airfoil thickness, camber ratio and performance was carried out. In conclusion, the high lift generating airfoils when compared to the reference case of the NACA 0012 airfoil, produce a velocity that is significantly higher, with or without the

5 flange, indicating that the overall setup is indeed more efficient and one that has a significant potential to be explored further.

5   References

[1] Ghenai,C., Salameh, T., Janajreh, I.: Modeling and Simulation of Shrouded Horizontal Axis Wind Turbine Using RANS Method. JJMIE. 11. ISSN 1995-6665. 2017.

[2] Dighe,V. V., Oliveira,G.de.: On the effects of the shape of the duct for ducted wind turbines, AIAA SciTech Forum. 2018.

10 [3] Dighe,V. V., Oliveira,G.de., Avallone,F., van Bussel G.J.W.: Towards improving the aerodynamic performance of a ducted wind turbine: A numerical study. Journal of Physics: Conf. Series, :10.1088/1742-6596/1037/2/022016, 2018. 16

[4] Ohya, Y., Karasudani, T., Sakurai, A., Abe, K-I., Inoue, M.:Development of a shrouded wind turbine with a flanged diffuser. Journal of Wind Engineering and Industrial Aerodynamics, 96(5), 524-539. https://doi.org/10.1016/j.jweia.2008.01.006, 2008.

[5] A. Aranake and K. Duraisamy: Aerodynamic optimization of shrouded wind turbines,

Wind Energ. (2016) DOI: 10.1002/we.2068

[6] Aly, M., El-Zahaby, Kabeel, A.,E., Elsayed., S.,S., Obiaa, M.,F.,: : CFD analysis of flow fields for shrouded wind turbine's diffuser model with different flange angles, Alexandria Engineering Journal (2016), https://doi.org/10.1016/j.aej.2016.08.036, 2017.

5 [7] Lilley, G.,M., Rainbird, W., J,: A preliminary report on the design and performance of ducted windmills Report No. 102, April, 1956.

[8] Igra, O.: Research and development for shrouded wind turbines, Energy Cont. Momt Vol. 21. pp. 13 to 48, https://doi.org/10.1016/0196-8904(81)90005-4, 1981

[9] Menter, F., R.,: Two-Equation Eddy-Viscosity Turbulence Models for Engineering Applications, AIAA JOURNAL Vol.
10 32,No. 8, August 1994

[10] Mikkelsen, R. F.: Actuator Disc Methods Applied to Wind Turbines, Kgs. Lyngby, Denmark: Technical University of Denmark (DTU). MEK-FM-PHD, No. 2003-02, 2004

[11] Suri, D.: Design of an Optimized Inlet Shroud for a Flanged Diffuser, 10.31224/osf.io/2qb6r, 2019.

[12] Radhakrishnan, J., and Suri, D.: Design and Optimisation of a Low Reynolds Number Airfoil for Small Horizontal Axis
15 Wind Turbines, IOP Conference Series: Materials Science and Engineering. Vol. 377. No. 1. IOP Publishing, doi:10.1088/1757-899X/377/1/012053, 2018

[13] Suri, D., Radhakrishnan, J., Nayak, R. (2019). Lattice Boltzmann Method to Analyse Fluid Flow Around a Circular Cylinder, 2019.

[14] Dighe, V., Suri, D., Avallone, F., and van Bussel, G.: Ducted wind turbines in yawed flow: A numerical study, Wind Energ.
20 Sci. Discuss., https://doi.org/10.5194/wes-2019-62, in review, 2019.

[15] "available at: https://climate.mit.edu/posts/potential-ducted-wind-turbines-urban-environment, 2019"

[16] "available at: https://www.gwec.net/wp-content/uploads/2015/03/GWEC$_{Global_W}ind_2014_Report_LR.pdf, 2018$]

[17] "available at: https://undocs.org/pdf?symbol=en/a/73/49(Vol.II), 2018"